



Analysis of Reinforced Concrete Beams by Finite Segment Technique

Hassan M. H. Ibrahim¹, Ibrahim A. El-Arabi² and. Moataz M. M. Rizk³

ABSTRACT

A finite segment numerical model, in the form of a computer program, for tracing the behavior of reinforced concrete (RC) beams from the initial loading stage up to failure is presented. The material nonlinear behavior is taken into account for both the concrete and reinforcing steel assuming perfect bond and linear strain distribution along the cross section. The effect of shear deformation is accounted for, while the torsional deformations and geometric nonlinearity are ignored. The load is applied incrementally and the equilibrium is ensured for every load step iteratively. The validity of the numerical model is established by comparing the predictions from the computer program with the response data acquired from published laboratory testing for several cases of simply supported beams with various dimensions. The comparison showed that the proposed model is suitable for simulating the bending behavior of simple beams (for a wide range of span to depth ratio); provided that an appropriate model for the reinforcing steel is chosen.

Keywords: Nonlinear analysis, reinforced concrete beam, shear deformation, and finite Segment Method.

الخلاصة باللغة العربية

تم اعداد نموذج رياضي (على هيئة برنامج حاسوبي) باستخدام طريقة القطعة المحددة للتنبؤ بالسلوك الإنشائي للكمرات الخرسانية المسلحة حتي الانهيار ، وتم أخذ السلوك غير الخطي لكل من الخرسانة وحديد التسليح في الاعتبار بفرض وجود تماسك كامل بينهما، ووجود توزيع خطي للانفعال على طول القطاع مع أخذ تأثير تشوهات القص في الحسبان. وقد أهمل التأثير الهندسي اللاخطي وكذلك تأثير تشوهات الالتواء. ويتم تطبيق الحمل بصورة تزايدية والتحقق من الاتزان بطرق تكرارية مع نهاية كل مرحلة للتحميل. وتم التحقق من صلاحية النموذج الرياضي المقترح بالمقارنة بنتائج التجارب المعملية المنشورة لحالات عديدة من الكمرات بسيطة الارتكاز بأبعاد مختلفة. وقد بينت المقارنة أن النموذج الرياضي المقترح مناسب للتنبؤ بسلوك الكمرات بسيطة الارتكاز المعرضة للانحناء وذلك لهجال كبير من نسب بحور الكمرات إلى أعماق قطاعاتها، ويتعين استخدام النموذج الأنسب لسلوك حديد التسليح.

1. Introduction

It is well known that the finite element method works well for analyzing steel structures, due to the straight forward constitutive behavior of the material. On the other hand, for materials such as concrete the behavior is basically nonlinear and much more complicated, which limits the capabilities of the finite element method in this latter case. The nonlinear response of RC is caused by two major effects, namely; cracking of concrete in tension, and yielding of the reinforcement or crushing of concrete in compression.

Many researches applied the finite element method to analyze RC beams. They discussed the finite element technique in two phases: 1) In-plane mesh technique [1-4] where the main concept of finite element model is to subdivide the domain of integration into a discrete number of small finite regions.

It will be possible to adopt simple functions to represent the local behavior of that region. 2) Finite segment technique [5-7] where the structural elements are divided into small segments. Every segment has a constant section property. It is assumed that the cracking in section means that the segment is fully cracked. Cross section properties can be determined by the (fiber model) [5 and 8] or (layered element model) [9 and 10]. In fiber or layered models, the models are based on satisfying equilibrium of stresses and compatibility of strains at all fibers of the cross-section.

The classical flexural beam theory cannot be used to understand the structural behavior of RC beams. Accordingly, there have been continuous experimental and analytical studies to investigate the behavior and develop design methods for RC beams.

Up till recent years, the behavior of RC beams under different circumstances still receiving the attention of many researchers. Kara and Dundar (2009) [11] prepared an analytical model to study the effect of loading types and reinforcement ratios on the stiffness and deflection of RC beams. Stramandinoli and La Rovere (2012) [12] presented a numerical model with the aim of capturing

¹ Professor of Concrete Structures, Head of Civil Engineering Department, Faculty of Engineering, Port Said University, Port Said, Egypt, E-mail: hi_hgh@yahoo.com

² Associate Professor, Civil Engineering Department, Faculty of Engineering, Port Said University, Port Said, Egypt, E-mail: iielarabiii@yahoo.com

³ Teaching Assistant, Civil Engineering Department, Faculty of Engineering, Port Said University, Port Said, Egypt, E-mail: moataz_m_rizk@yahoo.com

the combined shear and flexural behavior of RC beams, using a finite element model based on the Timoshenko Beam Theory. Based on the finite element method, different tension models were presented by Dede and Ayvaz (2009) [13] to compute the ultimate load capacity of RC beams. Some experimental investigations were carried out to study the behavior of high strength concrete beams failed in shear by Cladera and Marí (2005) [14].

The primary objective of the present study is to establish and demonstrate convenient, and reliable material models, and to develop a simple methodology for the nonlinear analysis of RC beams. The validity of the proposed models is verified by comparing the analytical predictions with results from previous experimental studies.

2. Numerical model

The proposed model to study the nonlinear behavior of RC sections under the effect of axial forces and bending moments is presented in this section. The model is based on satisfying both the equilibrium of stresses and compatibility of strains at all fibers of the cross-section.

2.1. Material models

In this study, bilinear stress-strain models are chosen for both the concrete in compression and reinforcing steel. The tension stiffening of concrete is also taken into consideration. All material models in the present work are extensively illustrated by Chen [15].

2.1.1. Concrete in compression

The material model for concrete in compression is shown in Fig. 1. In this case, the compressive stress is given by [15];

$$\sigma(\varepsilon_i) = \begin{cases} \varepsilon_i \times E_{c0} & \text{for } (0 \leq \varepsilon_i \leq \varepsilon_{c0}) \\ f_{cu} & \text{for } (\varepsilon_{c0} \leq \varepsilon_i \leq \varepsilon_{c \max}) \end{cases} \quad \dots\dots\dots (1)$$

$$\varepsilon_{c0} = f_{cu} / E_{c0}$$

$$\varepsilon_{c \max} = 0.0035$$

Where;

- $\varepsilon_{c \max}$ = Maximum concrete compression strain.
- ε_{c0} = Concrete compression yield strain.
- f_{cu} = Cubic compression strength after 28 day.
- E_{c0} = Concrete Young's modulus in elastic zone.

2.1.2. Concrete in tension

The stress-strain model for concrete in tension considering the tension stiffening effect is shown in Fig. 2. For that model [15];

$$\alpha = 6, \beta = 10, \gamma = (\alpha - 1) / \beta$$

$$\varepsilon_{Cr} = f_{Cr} / E_{c0}$$

$$\sigma(\varepsilon_i) = \begin{cases} \varepsilon_i \times E_{c0}, & 0 \leq \varepsilon_i \leq \varepsilon_{Cr} \\ E_{c0} \times (\varepsilon_i - \varepsilon_{Cr}) / \beta + \gamma \times f_{Cr}, & \varepsilon_{Cr} \leq \varepsilon_i \leq 6\varepsilon_{Cr} \end{cases} \quad \dots\dots\dots (2)$$

Where;

- α, β, γ = Concrete tension stiffening forming coefficient.
- ε_{Cr} = Concrete cracking strain.
- f_{Cr} = Concrete cracking stress.
- ε_{s0} = Steel yield strain.
- $\varepsilon_{s \max}$ = Maximum steel strain.
- ε_i = Strain of layer No. (i).

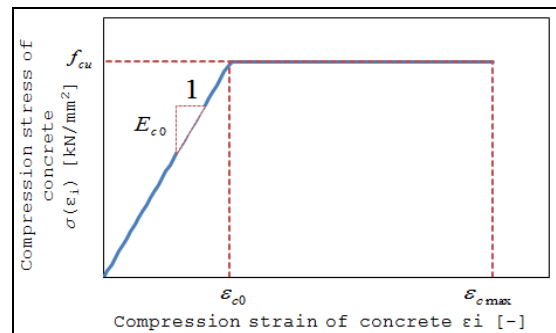


Figure 1: Stress-strain model of concrete in compression [15].

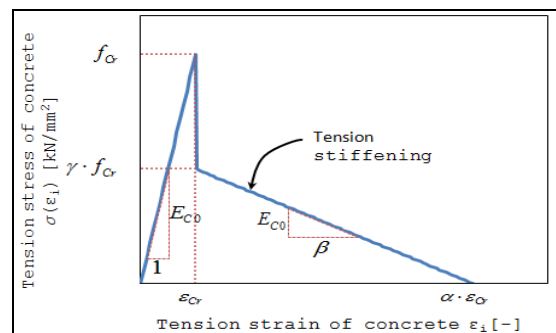


Figure 2: Stress-strain model of concrete in tension [15].

2.1.3. Steel models

The elastic-perfect plastic (EPP) stress-strain model for steel is shown in Fig. 3. In this case; the stress both in tension and compression is given by [15];

$$\sigma(\varepsilon_s) = \begin{cases} \varepsilon_s \times E_{s0}, & 0 \leq \varepsilon_s \leq \varepsilon_{s0} \\ f_y, & \varepsilon_{s0} \leq \varepsilon_s \leq \varepsilon_{s \max} \end{cases} \quad \dots\dots\dots (3)$$

$$\varepsilon_{s0} = f_y / E_{s0}$$

$$\varepsilon_{s \max} = 0.01$$

Where;

- ε_s = Steel strain.
- E_{s0} = Steel Young's modulus in elasticity zone.
- ε_{s0} = Steel yield strain.

$\varepsilon_{s\max}$ = Maximum steel strain.

f_y = Steel yield strength.

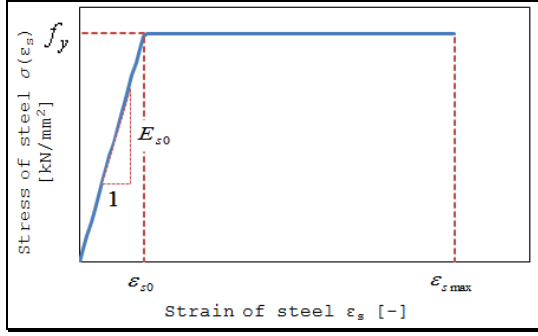


Figure 3: Stress-strain model of rebar [15].

The elastic-plastic hardening (EPH) model shown in Fig. 4 is appropriate for cold-worked steel reinforcement that doesn't exhibit a distinct yield plateau [15]. In this case;

$$\sigma(\varepsilon_s) = E_{s0} \times \varepsilon_s \times \left\{ A + \frac{1-A}{[1 + (B \times \varepsilon_s)^C]^{1/C}} \right\}, \dots \dots \dots (4)$$

$$A = \frac{E_{sh}}{E_{s0}}, B = \frac{E_{s0}(1-A)}{f_s^*}, C = 6, f_s^* = f_u - E_{sh} \times \varepsilon_u$$

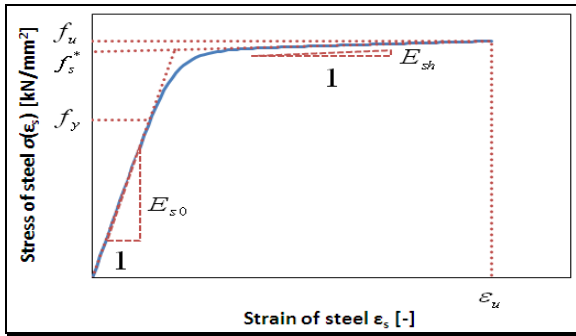


Figure 4: Stress-strain model for rebar [15].

2.2. Reinforced concrete section model

The proposed numerical model for nonlinear analysis of a RC section subjected to an axial load N_z and bending moment M_x is presented herein. The model is based on the following assumptions:

- 1) Strain distribution is assumed to be linear along the section while the stress distribution is nonlinear.
- 2) Perfect bond between concrete and reinforcing steel is assumed.
- 3) Deformation due to torsion is neglected.
- 4) The effect of geometric nonlinearity is not considered.

The main objective of the model is to find the effective area A and moment of inertia I_z of the RC section. Referring to Fig. 5, the sectional computations are carried out as follows:

- 1) Initially, compute the coefficients of axial (EA) and bending (EI) rigidities for the concrete section neglecting the reinforcement, and locate the initial position of the neutral axis, as

$$\begin{aligned} EA &= E_{C0} \times b \times t \\ EI &= E_{C0} \times b \times t^3 / 12 \dots \dots \dots (5) \\ \bar{y} &= t / 2 \text{ (from upper fiber)} \end{aligned}$$

- 2) Calculate the strain ε at both the top and bottom edges of the section and locate the position of the neutral axis NAL , as

$$\begin{aligned} \varepsilon_{top} &= N_z / EA - M_x / EI \times \bar{y} \\ \varepsilon_{bot} &= N_z / EA + M_x / EI \times (t - \bar{y}) \dots \dots \dots (6) \\ NAL &= \varepsilon_{top} / (\varepsilon_{top} - \varepsilon_{bot}) \times t \end{aligned}$$

- 3) Divide the section into a number of identical layers with a width b and a constant depth dy . Then, calculate the strain at every layer depending on its distance y_i from the top edge of the section. Steel strains both in tension and compression are to be computed too; depending on the distances d and Dd from the upper edge, respectively.

$$\begin{aligned} dy &= t / n_{Layers} \\ y_i &= dy / 2 + dy \times (i - 1) \\ \varepsilon_i &= \varepsilon_{top} \times (NAL - y_i) / NAL \dots \dots \dots (7) \\ \varepsilon_{ComSt} &= \varepsilon_{top} \times (NAL - Dd) / NAL \\ \varepsilon_{TenSt} &= -\varepsilon_{top} \times (d - NAL) / NAL \end{aligned}$$

- 4) Calculate the stress and elasticity modulus E_C for every concrete layer, as well as for the steel layers resulting from the computed strains.

$$\begin{aligned} E_C(i) &= d\sigma_C(\varepsilon_i) / d\varepsilon \\ E_{ComSt} &= d\sigma_S(\varepsilon_{ComSt}) / d\varepsilon \dots \dots \dots (8) \\ E_{TenSt} &= d\sigma_S(\varepsilon_{TenSt}) / d\varepsilon \end{aligned}$$

- 5) Calculate the overall section properties, as

$$\begin{aligned} EA_{St} &= E_{ComSt} \times CA_s + E_{TenSt} \times TA_s \\ EA &= EA_{St} + b \times dy \times \sum_{i=1}^{n_{Layers}} E_C(\varepsilon_i) \dots \dots \dots (9) \end{aligned}$$

$$EA_{St} \times y_{St} = E_{ComSt} \times CA_s \times Dd + E_{TenSt} \times TA_s \times d$$

$$\bar{y} = \left(EA_{St} \times y_{St} + b \times dy \times \sum_{i=1}^{n_{Layers}} y_i \times E_C(\varepsilon_i) \right) / EA$$

$$EI_C = \sum_{i=1}^{n_{Layers}} E_C(\varepsilon_i) \times (b \times dy^3 / 12 + b \times dy \times y_i^2) \quad (10)$$

$$\begin{aligned} EI_S &= E_{ComSt} \times CA_s \times Dd^2 + E_{TenSt} \times TA_s \times d^2 \\ EI &= EI_C + EI_S - EA \times \bar{y}^2 \end{aligned}$$

- 6) Solution steps from 2 to 5 are repeated with the most updated section properties, until an error tolerance of 0.01 for both EA and EI is achieved; provided that the compression strain of concrete at the top edge does not exceed 0.0035.

- 7) Compute the effective section area A and inertia moment I_z , as
- 8) $A = EA/E_C$ (11)
 $I_z = EI/E_C$

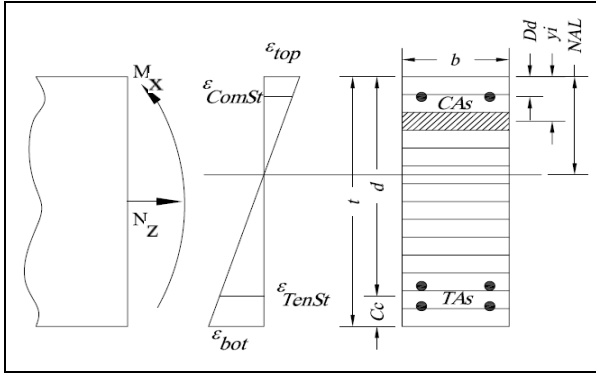


Figure 5: The Section Layered Model.

A and I_z are computed at the start and end for every segment, then the average values are taken as the segmental properties that will be used in the subsequent steps of the analysis.

2.3. Force-Displacement Relationship

2.3.1. Element stiffness in local coordinates

Referring to Fig. 6-a, the force displacement relationship of a plane frame element in local coordinates is expressed as $\{F\} = [K]\{\delta\}$ where;

$$[K] = \frac{EA}{L} \begin{bmatrix} 1 & 0 & 0 & -1 & 0 & 0 \\ 0 & \frac{12I}{AL^2} & \frac{6I}{AL} & 0 & \frac{-12I}{AL^2} & \frac{6I}{AL} \\ 0 & \frac{6I}{AL} & \frac{4I}{A} & 0 & \frac{-6I}{AL} & \frac{2I}{A} \\ -1 & 0 & 0 & 1 & 0 & 0 \\ 0 & \frac{-12I}{AL^2} & \frac{-6I}{AL} & 0 & \frac{12I}{AL^2} & \frac{-6I}{AL} \\ 0 & \frac{6I}{AL} & \frac{2I}{A} & 0 & \frac{-6I}{AL} & \frac{4I}{A} \end{bmatrix},$$

$$\{F\}^T = \{F_{x_1} \quad F_{y_1} \quad M_{z_1} \quad F_{x_2} \quad F_{y_2} \quad M_{z_2}\}, \text{ and}$$

$$\{\delta\}^T = \{u_1 \quad v_1 \quad \theta_1 \quad u_2 \quad v_2 \quad \theta_2\} \dots \dots \dots (12)$$

According to Dundar and Kara [16], the stiffness matrix $[K]$ can be modified to consider the effects of shear deformations as follows:

$$[K] = \frac{E}{L} \begin{bmatrix} A & 0 & 0 & -A & 0 & 0 \\ 0 & \frac{12I}{L^2\Omega_{z1}} & \frac{6I}{L\Omega_{z1}} & 0 & \frac{-12I}{L^2\Omega_{z1}} & \frac{6I}{L\Omega_{z1}} \\ 0 & \frac{6I}{L\Omega_{z1}} & \frac{4I}{\Omega_{z2}} & 0 & \frac{-6I}{L\Omega_{z1}} & \frac{2I}{\Omega_{z3}} \\ -A & 0 & 0 & A & 0 & 0 \\ 0 & \frac{-12I}{L^2\Omega_{z1}} & \frac{-6I}{L\Omega_{z1}} & 0 & \frac{12I}{L^2\Omega_{z1}} & \frac{-6I}{L\Omega_{z1}} \\ 0 & \frac{6I}{L\Omega_{z1}} & \frac{2I}{\Omega_{z3}} & 0 & \frac{-6I}{L\Omega_{z1}} & \frac{4I}{\Omega_{z2}} \end{bmatrix} \quad (13)$$

Where;

$$\Omega_{z1} = 1 + \varphi_z, \Omega_{z2} = 4 \frac{1 + \varphi_z}{4 + \varphi_z},$$

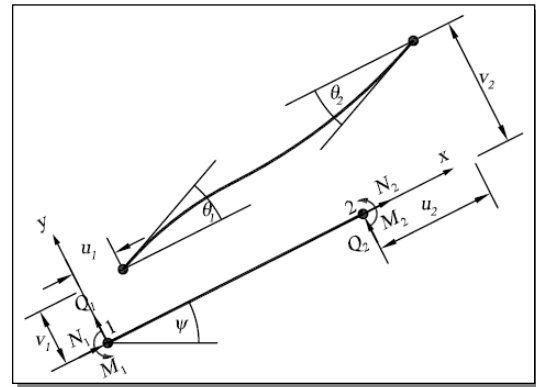
$$\Omega_{z3} = 2 \frac{1 + \varphi_z}{2 - \varphi_z}, \text{ and } \varphi_z = \frac{12EI}{G_{eff}AL^2} = \text{Shear angle}$$

As shown in Table 1, the effective shear modulus G_{eff} depends on the type of RC element, [16].

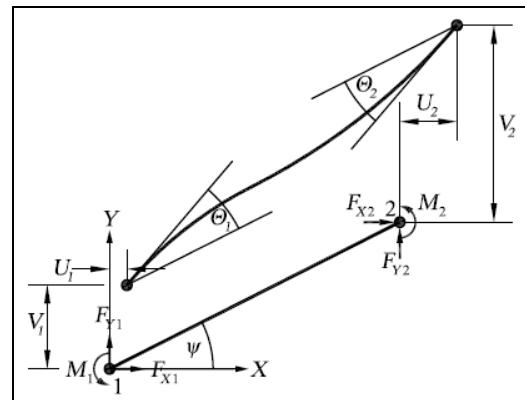
Table 1: Effective shear modulus G_{eff} for RC elements, [16].

Element type	Effective shear modulus
Beams and frames	$G_{eff} = \begin{cases} 0.24G_c(1 - 250\varepsilon_i), & \varepsilon_i \geq \varepsilon_{Cr} \\ G_c, & \varepsilon_i < \varepsilon_{Cr} \end{cases}$
Deep beams	$G_{eff} = 0.25G_c$
Shear walls	$G_{eff} = 0.125G_c$

$G_c = E_c / (2(1 + \nu))$ and $\nu = \text{Poisson's ratio} = 0.2$ for RC.



a) Local coordinate system.



b) Global coordinate system.

Figure 6: Coordinate systems

2.3.2. Global element stiffness matrix

The local stiffness matrix $[K]$ can be transformed into its global form $[\bar{K}]$ with respect to the global coordinates shown in Fig. 6-b. This can be achieved by the multiplication by the transformation matrix $[Tr]$ as

$$[\bar{K}] = [Tr]^T [K] [Tr] \dots \dots \dots (14)$$

And;

$$[Tr] = \begin{bmatrix} \cos \psi & \sin \psi & 0 & 0 & 0 & 0 \\ -\sin \psi & \cos \psi & 0 & 0 & 0 & 0 \\ 0 & 0 & 1 & 0 & 0 & 0 \\ 0 & 0 & 0 & \cos \psi & \sin \psi & 0 \\ 0 & 0 & 0 & -\sin \psi & \cos \psi & 0 \\ 0 & 0 & 0 & 0 & 0 & 1 \end{bmatrix} \dots (15)$$

Moreover, the global load and displacement vectors ($\{\bar{F}\}$ and $\{\bar{\delta}\}$) are related to the local load and displacement vectors through

$$\begin{aligned} \{\bar{F}\} &= [Tr]^T \{F\} \\ \{\bar{\delta}\} &= [Tr] \{\delta\} \end{aligned} \dots (16)$$

2.4. Iterative solution

The nonlinear nature of the force displacement relationship requires an iterative solution procedure. The computations in this work are carried out using a linear stepwise load-incremental method. The load is applied in a series of small increments, and for each of these increments, the changes in deformations and internal forces are determined. The tangent stiffness matrix, based on the values of axial and flexural rigidities existing at the beginning of any step, is used to calculate the change in the deformation caused by the load increment. Mathematically, this can be expressed as

$$[K_T] \{\Delta\delta\} = \{\Delta F\} \dots (17)$$

Where; $[K_T]$ is the tangential stiffness matrix, $\{\Delta\delta\}$ is the incremental displacement vector, $\{\Delta F\}$ is the incremental nodal force vector. The tangential stiffness matrix $[K_T]$ can be written as:

$$[K_T] = \sum_{i=1}^{i=n} [K_i] \dots (18)$$

Where; $[K_i]$ is the element stiffness matrix, the subscript i refers to the element number, and n is the number of elements. The total displacements and internal forces existing at the end of any step are obtained by summing the incremental changes in displacements and internal forces up to the end of that step. At the ultimate load the stiffness matrix will be singular and the structure will no longer be stable. A summary of the linear incremental method is listed below: Specify the incremental loads $\{\Delta F\}$.

- 1) Using the axial and flexural rigidities (as explained in Sec. 2.2), form the local stiffness matrix $[K]$ for each element and construct the transformation matrix $[Tr]$.
- 2) Transform the element stiffness matrix from local to global coordinates and combine to form the overall stiffness matrix $[K]$.
- 3) Solve for the incremental displacement $\{\Delta\delta\}$ using Eq. (17).
- 4) Using $\{\Delta\delta\}$, determine the change in internal forces $\{\Delta P\}$.

- 5) Calculate the total value of $\{\delta\}$, $\{P\}$ and $\{F\}$ by adding the increments to the existing quantities.
- 6) Return to step 2 for the next load increment.

2.5. Sensitivity analysis

An open source computer program called NAFS was especially written to trace the nonlinear response of RC beams up to failure by finite segment technique. The program code involves all above-mentioned constitutive models, formulations, and solution procedures. A sensitivity study is carried out in this section to find the optimum segment size for the proposed numerical model. The solution technique and computer program will then be verified in the next sections against some previously published test results. A flowchart is given in the Appendix to illustrate the main steps used to find the RC element properties using the finite segment model.

The simple beam tested earlier by dePaiva and Austin, [17] under a uniform load, is reanalyzed by the current model considering different element sizes and the results are shown in Fig. 7. The abscissa in Fig. 7 shows the number of elements used to model one half only of the symmetric beam; while the coordinate shows both the midspan deflection [mm] and the scalable ultimate load capacity [kN]. It can be seen that the ultimate load is less sensitive to the variations in segment size; when compared with the midspan deflection. The acceptable results of the central deflection could only be achieved when 10 (as an average value) elements were used to model one half the span. For all cases under investigation in this study, the full model of a simple beam comprises a total of 20 finite segments as shown in Fig. 8.

3. Verification of the model

In most of current codes of practice, RC beams are classified as deep or slender beams according to their span-to-depth (L/d) ratios. For instance, the span of a deep beam in ACI 318-08 [18] should not exceed four times the overall member depth. The Eurocode-1992 [19] defines the deep beam as a beam whose span is equal to or less than 3 times the overall section depth. The Egyptian code (ECP 203) [20] defines the deep beam as a beam for which the L/d ratio is less than or equal 2.0 for a simple beam, and less than or equal 2.5 for a continuous beam.

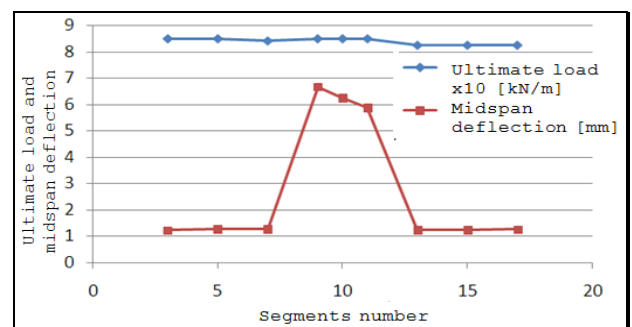


Figure 7: Effect of segments size on results.

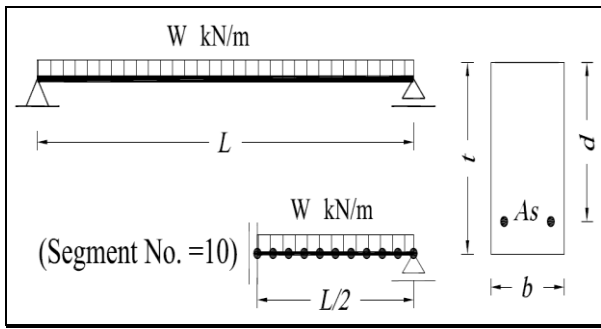


Figure 8: Typical simply supported beam and segment divisions into 10 segments.

Verifications are performed in this section for the following three categories: (1) Two deep beams for which $L/d \leq 2$; (2) Two short beams for which $2 < L/d < 4$; and (3) Four slender beams for which $4 \leq L/d \leq 11$. The simply supported RC beam shown in Fig. 8, which is subjected to a uniform load, was tested earlier by many researchers [1, 17, and 21]. The dimensions and design parameters for the tested beams are listed in Table 2. The main reinforcement of the cross section as well as the material properties vary as shown. All cases of tested beams failed in flexure. The experimental results for those beams are compared in Tables 3 and 4 with the theoretical results obtained by the present model.

Referring to Table 3, the ultimate load capacities W_{test} given in the 2nd column were found by the tests; while the W_u results given in the 3rd to the 6th column were calculated numerically by the present model. The corresponding midspan deflections are listed in Table 4. Four different constitutive models for the reinforcing steel were examined with the proposed model, as it is illustrated below Table 3. For the sake of comparison, the predicted results W_u and δ_u were normalized using the ultimate test results W_{test} and δ_{test} , respectively, in each case. The normalized results are listed in the 7th through the 10th column in Tables 3 and 4. The theoretical ultimate load predictions W_u were calculated based on EPH and EPP models, described earlier in Sec. (2.1), with material parameters as given in Table 2. However, for W_u computed on the basis of EPHEC and EPPEC models, the stress levels given in Table 2 for both the concrete and rebar were limited to the design parameters and strength reduction factors recommended by ECP 203 Code [20]. This means that concrete characteristic strength is reduced to 45% of its original value; whereas the yield strength of reinforcement is reduced by 13%. Figures 9 through 16 show the comparisons between load-deflection curves for the midspan section in every case, as obtained experimentally and numerically considering the different steel models.

3.1. Deep beams ($L/d \leq 2$):

As shown in Figs 9 and 10, the theoretical and experimental results are in excellent agreement up till 50% of the test ultimate load. Although all theoretical models showed stiffer behaviors for further loading, yet

the ultimate load predictions for some of the theoretical models (such as the plastic hardening EPH and EPHEC models) are in good agreement with the test results. For deep beams, the EPH ultimate load predictions were found to agree with the test results with maximum discrepancies of 13%, as given in Table 3. Moreover, the EPHEC ultimate load predictions were found to agree with the test results with maximum discrepancies of 21%. Load discrepancies increase up to 32% and 37% for the elastic-perfect plastic EPP and EPPEH models, respectively. However, the proposed model, as listed in Table 4, was too stiff such that it could not give any satisfactory predictions for the deflection, in this case.

3.2. Short beams ($2 < L/d < 4$):

Figures 11 and 12 describe the theoretical and experimental load-deflection response for two short beams of 2.66 and 3.71 span-to-depth ratios, respectively. As shown by the two figures, although different models were used for the rebar, the theoretical load-deflection behaviors are very close to one another, and agree well with the test results, up till 85% of W_{test} . For further loading, both plastic hardening models of rebar (i.e. EPH and EPHEC) showed stiffer behaviors, whereas both elastic-perfect plastic models (i.e. EPP and EPPEC) showed more realistic behaviors. For both test beams, the most accurate theoretical predictions were also achieved via the elastic-perfect plastic models, as given in Table 2. For $L/d = 2.66$, the EPP model gave a zero error prediction, whereas the percentage error in the EPPEC prediction was 12% lower than W_{test} . For the other short beam ($L/d = 3.71$), the predictions of the same two models (EPP and EPPEC), respectively, were 26% and 11% higher than W_{test} . On the other hand, the EPH and EPHEC predictions were 21% and 9%, respectively, higher than W_{test} for $L/d = 2.66$. For $L/d = 3.71$, the discrepancy was much more noticeable and reached 83% and 56% higher than W_{test} , for the EPH and EPHEC predictions, respectively.

As listed in Table 4, the deflection predictions still underestimate, if compared with the test results. However, the situation in this case is much better, if compared with deep beams. Elastic perfect plastic models show a relative more flexible response compared to the elastic plastic hardening models, in this case.

3.3. Slender beams ($4 \leq L/d \leq 11$):

The theoretical and experimental load-deflection responses for 4-slender beams are depicted in Figs 13 through 16. The span-to-depth ratio for the 4-beams is 4, 6, 8.8, and 11, respectively. It can be seen from the figures that all theoretical load-deflection behaviors are stiffer, if compared with the corresponding experimental behavior. However, they are very close to one another for every tested beam. For beams with $L/d = 4$ to 6, this typical coincidence of the load-deflection curves continues along the entire loading history until the full experimental ultimate capacity W_{test} is reached. For $L/d = 8.8$ and 11, respectively, it continues up till 97% and 85% of W_{test} . This means that a conservative estimation

of the ultimate capacity W_u for a slender beam ($L/d \geq 4$) can be obtained throughout the proposed model. In this case, the load-deflection response of the beam is to be plotted by the 4-proposed models. The first point at which the theoretical response curves deviate from one another is to be determined. Then, the load level at the deviation point can be taken as a conservative estimation of the ultimate capacity of the beam.

For deflection predictions, it can also be seen from Figs 9 to 16 that the proposed models are more efficient for

slender beams if compared with short and deep beams. Deflection estimations at failure are much closer to the test results for slender beams; especially for the elastic-perfect plastic EPP and EPPEC models. Among the proposed models, the EPPEC model can be considered as the best for nonlinear analysis of slender beams; because the response curves achieved by that model are the closest to the test results. The greater the span-to-depth L/d ratio, the closer the theoretical predictions of deflection to test results.

Table 2: The dimensions and design parameters of tested beams.

Beam	Ref.	L/d	L [mm]	d [mm]	t [mm]	b [mm]	$Rft.$ [mm ²]	f_{cu} [MPa]	f_{tu} [MPa]	E_c [GPa]	f_y [MPa]	E_s [GPa]
NLB1.0	[17]	1.0	914	914	959	114	258	35	3.5	26	331	210
NLB2.0	[17]	2.0	914	457	503	114	400	34	3.5	25.7	307	210
NLB2.66	[1]	2.66	2473	931	991	203	2443	17	2.3	18.1	320	210
NLB3.71	[1]	3.71	2438	657	686	203	1927	22.5	2.1	20	350	206
NLB4.0	[17]	4.0	914	229	273	114	258	24	2.9	21.6	334	210
NLB6.0	[17]	6.0	914	152	195	114	142	29	3.2	23.7	382	210
NLB8.8	[21]	8.8	2235	253	305	152	852	43	3.9	28.9	305	210
NLB11.0	[21]	11.0	2794	252	305	152	387	36	3.6	26.4	462	210

Table 3: The experimental and theoretical ultimate load capacities of tested beams.

Beam	W_{test} [kN/m]	Ultimate Load W_u [kN/m]				W_u/W_{test} [--]			
		EPH ¹	EPHEC ²	EPP ³	EPPEC ⁴	EPH	EPHEC	EPP	EPPEC
NLB1.0	1236	1171	982	841	776	0.95	0.79	0.68	0.63
NLB2.0	751	851	742	562	498	1.13	0.99	0.75	0.66
NLB2.66	743	901	808	743	656	1.21	1.09	1.00	0.88
NLB3.71	308	564	481	388	343	1.83	1.56	1.26	1.11
NLB4.0	173	313	265	213	189	1.81	1.53	1.23	1.09
NLB6.0	74	144	122	98	85	1.95	1.65	1.32	1.15
NLB8.8	103	174	148	120	106	1.69	1.44	1.17	1.03
NLB11.0	51	71	63	55	49	1.39	1.24	1.07	0.95

¹ EPH = Elastic Plastic Hardening steel stress-strain model.

² EPHEC = Elastic Plastic Hardening steel stress-strain model considering the design parameters and strength reduction factors for concrete and steel reinforcement adopted by ECP 203 Code.

³ EPP = Elastic Perfect Plastic steel stress-strain model.

⁴ EPPEC = Elastic Perfect Plastic steel stress-strain model considering the design parameters and strength reduction factors for concrete and steel reinforcement adopted by ECP 203 Code.

Table 4: The experimental and theoretical deflection at midspan of tested beams.

Beam	δ_{test} [mm]	Midspan deflection δ_u [mm]				δ_u/δ_{test}			
		EPH	EPHEC	EPP	EPPEC	EPH	EPHEC	EPP	EPPEC
NLB1.0	18.1	1.21	1.13	0.59	0.48	0.07	0.06	0.03	0.03
NLB2.0	21.8	2.15	1.89	0.85	0.73	0.10	0.09	0.04	0.03
NLB2.66	20.0	7.78	8.07	9.40	1.10	0.39	0.40	0.47	0.51
NLB3.71	19.9	7.97	8.78	8.68	11.80	0.40	0.44	0.44	0.59
NLB4.0	10.5	3.53	3.23	2.89	3.10	0.34	0.31	0.28	0.30
NLB6.0	15.2	4.90	4.41	5.80	6.23	0.32	0.29	0.38	0.41
NLB8.8	27.0	16.60	17.10	26.00	32.30	0.61	0.63	0.96	1.20
NLB11.0	51.1	33.90	36.00	51.10	105.50	0.66	0.70	1.00	2.06

4. Conclusions and Recommendations

A nonlinear analysis of RC beams based on finite segment technique and a direct iterative solution scheme was presented. The presented model takes account for material nonlinearities of concrete (both in tension and compression) and rebar, assuming perfect bond and linear strain distribution along the cross section. Four

different nonlinear material models for rebar were considered. The present analysis has the advantage to easily trace the nonlinear response of RC flexure beams along the entire monotonic load history up till failure. The analysis accuracy and efficiency was validated against 8-cases of deep, short, and slender test beams from the literature. From the comparisons and analyses carried out in this work, the following could be drawn:

- a) Several times, the proposed model could successfully trace the nonlinear response of RC deep, short, and slender flexure beams subjected to monotonic loads up to failure.
- b) The model can satisfactorily predict the ultimate load capacity for deep beams ($L/d \leq 2$) and short beams ($2 < L/d < 4$) using the elastic-plastic

hardening EPH and EPHEC models. The EPH model is more suitable for deep beams with L/d closer to 1, while the EPHEC model gives better predictions as L/d ratio is closer to 2. However, the deflection predictions are not acceptable for both models.

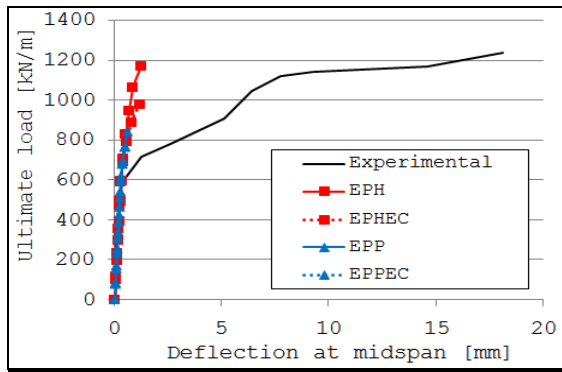


Figure 9: Distributed load vs. midspan deflection for beam with $L/d = 1$.

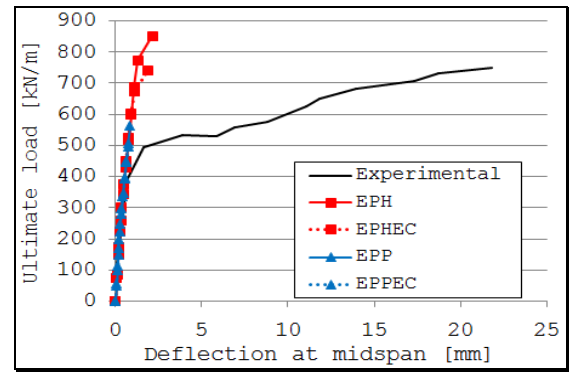


Figure 10: Distributed load vs. midspan deflection for beam with $L/d = 2$.

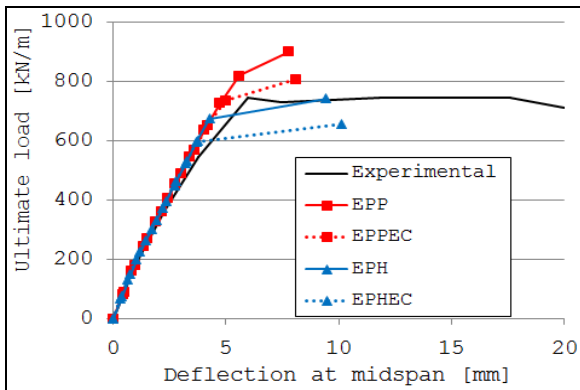


Figure 11: Distributed load vs. midspan deflection for beam with $L/d = 2.66$.

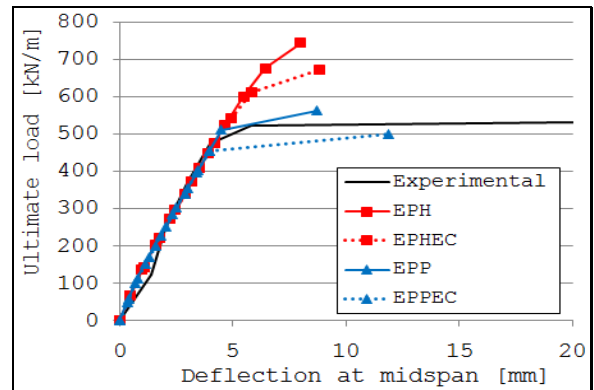


Figure 12: Distributed load vs. midspan deflection for beam with $L/d = 3.71$.

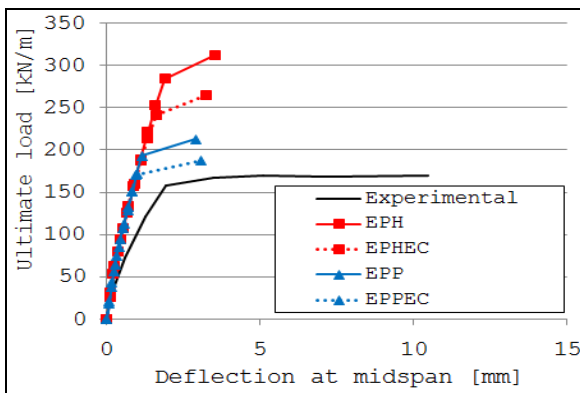


Figure 13: Distributed load vs. midspan deflection for beam with $L/d = 4$.

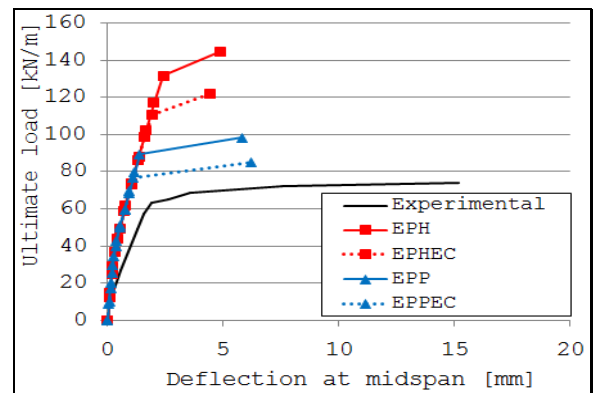


Figure 14: Distributed load vs. midspan deflection for beam with $L/d = 6$.

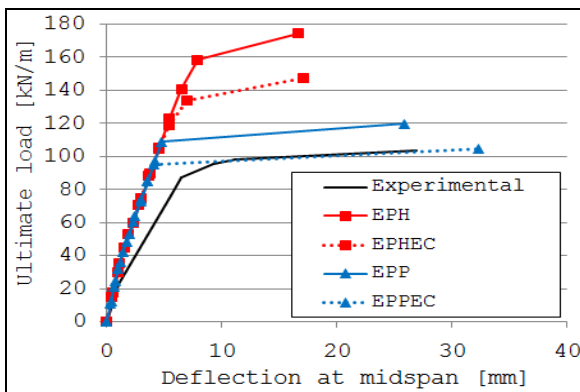


Figure 15: Distributed load vs. midspan deflection for beam with $L/d = 8.8$.

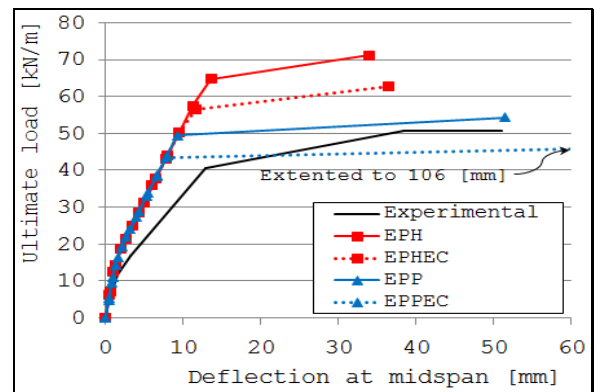


Figure 16: Distributed load vs. midspan deflection for beam with $L/d = 11$.

- c) For short beams ($2 < L/d < 4$), the model can satisfactorily predict the ultimate load capacity using the elastic-perfect plastic EPP and EPPEC models. The EPP model is more suitable for short beams with L/d closer to 2, while the EPPEC model gives better predictions as L/d ratio is closer to 4. The deflection predictions are much better than those of deep beams but they still underestimate for all models, in this case too.
- d) The proposed model can satisfactorily predict the ultimate load capacity (within 11% of the test results) for slender beams, via elastic-perfect plastic EPPEC model. However, the deflection predictions are irregularly accurate.
- e) A conservative estimation of the ultimate capacity W_u for short and slender beams (within 15%) can easily be obtained throughout the proposed model. This estimation can be encountered at the first point of deviation obtained from the plot of the 4-theoretical response curves computed by the 4-proposed models.

References

- [1] Ibraheim, H. M. H. "Application of the Finite Element Method to Reinforced Concrete Structures", *M.Sc.*, Civil Engineering Dept., Faculty of Engineering, Suez Canal University, 1991.
- [2] Zaki, Sh. M. "Nonlinear Analysis Monotonic and Cyclic Response of Reinforced Concrete Structures Containing Shear Walls", *Ph.D.*, Civil Engineering Dept., Faculty of Engineering, Suez Canal University, 2007.
- [3] Slobbe, A.T., Hendriks, M. A. N., and Rots, J. G. "Sequentially Linear Analysis of Shear Critical Reinforced Concrete Beams Without Shear Reinforcement", Faculty of Civil Engineering and Geosciences, Delft University of Technology, 2011.
- [4] Hengprathanee, S. "Linear And Nonlinear Finite Element Analyses of Anchorage Zones in Post-Tensioned Concrete Structures", *Ph.D.*, Blacksburg, Virginia, 2004.
- [5] El-Sabbagh, A. I. "Nonlinear Cyclic Dynamic Behavior of Composite Structures", *Ph.D.*, Civil Engineering Dept., Faculty of Engineering, Suez Canal University, 2007.
- [6] Breysse, D., and Mazars, J. "Simplified Approach of Nonlinearity in R-C Beams", *Journal of Structural Engineering*, Vol. 114, No. 2, Feb. 1995, ASCE.
- [7] Kandil, O. A. "Nonlinear Analysis of Reinforced Concrete Structures", *M.Sc.*, Civil Engineering Dept., Faculty of Engineering, Suez Canal University, 2006.
- [8] Valipour, H. R., and Foster, S. J. "A Total Secant Flexibility Based Formulation for Frame Elements with Physical and Geometrical Nonlinearities", Centre for Infrastructure Engineering and Safety (CIES), School of Civil and Environmental Engineering, The University of New South Wales, Sydney 2052, Australia, 2009.
- [9] Ramaswamy, A., Barzegar, F., and Voyiadjis, G. Z. "Study of Layering Procedures in Finite-Element Analysis of RC Flexural and Torsional Elements", *Journal of Structural Engineering*, Vol. 121, No. 12, December 1995, ASCE.
- [10] Oliveira, R.S., Ramalho, M.A., and Corrêa, M. R. S. "A Layered Finite Element for Reinforced Concrete Beams with Bond-Slip Effects", Elsevier Ltd., www.elsevier.com, 2007.
- [11] Kara, I. F., and Dundar, C. "Effect of Loading Types and Reinforcement Ratio on An Effective Moment of Inertia and Deflection of A Reinforced Concrete Beam", *Advances in Engineering Software*, 40 (2009) 836–846, www.elsevier.com.
- [12] Stramandinoli, R. S. B., and La Rovere, H. L. "FE Model for Nonlinear Analysis of Reinforced Concrete Beams Considering Shear Deformation", *Engineering Structures* 35 (2012) 244–253, www.elsevier.com.
- [13] Dede, T., and Ayvaz, Y. "Nonlinear analysis of reinforced concrete beam with/without tension stiffening effect", *Materials and Design* 30 (2009) 3846–3851, www.elsevier.com.
- [14] Cladera, A., and Marí, A. R. "Experimental study on high-strength concrete beams failing in shear", *Engineering Structures* 27 (2005) 1519–1527, www.elsevier.com.
- [15] Chen, W.F., (1982). "Plasticity in Reinforced Concrete." McGraw-Hill.
- [16] Dundar, C., and Kara, I. F. "Three dimensional analysis of reinforced concrete frames with cracked beam and column elements", *Ph.D.*, Department of Civil Engineering, Cukurova University, 01330, Adana, Turkey, Nov. 2006.
- [17] dePaiva, H. A., and Austin, W. J. "Behavior and Design of Deep Structural Members, Part 3: Tests of Reinforced Concrete Deep Beams", University of Illinois, Urbana, March 1960, Structural Research Series SRS-194.
- [18] American standard, Building Code Requirements for Structural Concrete and Commentary (ACI 318-08), American Concrete Institute, 2008.
- [19] Euro-code 2, Design of Concrete structure

(EN1992-1-1), European Committee for Standardization.

- [20] Egyptian Code of Practice for Design and Construction of Reinforced Concrete Structures, Code No. 203, 2010.
- [21] Bernaert, S., and Siess, C. P. "Strength in Shear of Reinforced Concrete Beams Under Uniform Load", University of Illinois, Urbana, June 1956, Structural Research Series SRS-120.

Appendix I: Flowchart

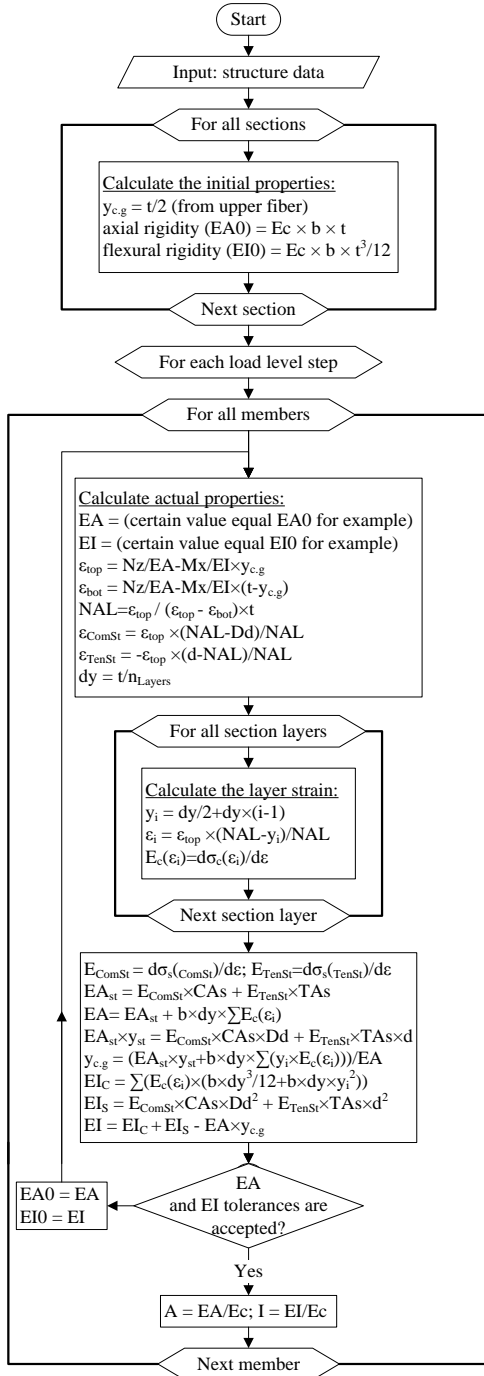


Figure A.1: Flowchart illustrates the main steps used to find the RC element properties using the finite segment

model.

Appendix II: Notations

The following symbols are used in this paper:

- α, β, γ = Concrete tension stiffening forming coefficients.
- ϵ_{c0} = Concrete compression yield strain.
- ϵ_{cmax} = Maximum concrete compression strain.
- ϵ_{cr} = Concrete cracking strain.
- ϵ_{s0} = Steel yield strain.
- ϵ_{smax} = Maximum steel strain.
- ϵ_i = Strain of layer No. (i).
- ϵ_{top} = Cross section top fiber strain.
- ϵ_{bot} = Cross section bottom fiber strain.
- ϵ_{ComSt} = Strain of compression steel.
- ϵ_{TenSt} = Strain of tension steel.
- ν = Poisson's ratio.

$\Omega_{z1}, \Omega_{z2}, \Omega_{z3}$ = Shear deformation coefficients.

φ_z = Shear angle.

b = Width of RC section.

d = Distance of tension steel from upper fiber.

$f(\epsilon_i)$ = Stress function of concrete layer No. (i).

$f(\epsilon_s)$ = Stress function of rebar row.

f_{cr} = Concrete cracking stress.

f_{cu} = Cubic concrete compression stress after 28 days.

f_y = Steel yielding stress.

dy = Concrete layer thickness.

\bar{y} = Cross section gravity center position (from upper fiber).

y_i = Distance between center of layer (i) and upper fiber.

t = Overall depth of RC section.

A = Cross-section area.

CAs = Compression steel area.

Dd = Distance of compression steel from upper fiber.

E_{c0} = Concrete Young's modulus in elasticity zone.

E_{s0} = Steel Young's modulus in elasticity zone.

EA, EI = Axial and flexural rigidities of cross section.

$E_c(i)$ = Elasticity modulus of concrete layer No. (i).

E_{ComSt} = Elasticity modulus of compression steel.

E_{TenSt} = Elasticity modulus of tension steel.

EA_{St} = Total steel axial rigidity.

EI_C = Concrete flexural rigidity.

EI_S = Steel flexural rigidity.

- G_c, G_{eff} = Shear modulus and Effective shear modulus.
 I_z = Cross-section moment of inertia.
 L = Segment element length.
 NAL = Neutral axis location (from upper fiber).
 TAs = Tension steel area.
 $\{\delta\}$ = Nodal displacement vector in local coordinate system.
 $\{F\}$ = Nodal force vector in local coordinate system.
 $\{\bar{\delta}\}$ = Nodal displacement vector in global coordinate system.
 $\{\bar{F}\}$ = Nodal force vector in global coordinate system.
 $[K]$ = Stiffness matrix in local coordinate system.
 $[\bar{K}]$ = Stiffness matrix in global coordinate system.
 $\{P\}$ = The applied nodal loads vector at free degrees of freedom.
 $\{R\}$ = The reactions or resulting forces vector at restrained degrees of freedom.
 Rtf = Reinforcement.
 $[Tr]$ = Transformation matrix.
 $\{U_f\}$ = The displacement vector at free degrees of freedom.
 W_{test} = Experimental failure load.
 W_u = Ultimate load computed by model.
 δ_{test} = Experimental deflection at failure.
 δ_u = Deflection at ultimate load computed by model.